

# HRSeg: High-Resolution Visual Perception and Enhancement for Reasoning Segmentation

Weihuang Lin<sup>1\*</sup>, Yiwei Ma<sup>1\*</sup>, Xiaoshuai Sun<sup>1†</sup>, Shuting He<sup>2</sup>, Jiayi Ji<sup>1</sup>, Liujuan Cao<sup>1</sup>,  
Rongrong Ji<sup>1</sup>

<sup>1</sup>Key Laboratory of Multimedia Trusted Perception and Efficient Computing, Ministry of Education of China,  
Xiamen University, 361005, P.R. China,

<sup>2</sup>Shanghai University of Finance and Economics

## Abstract

The reasoning segmentation task involves segmenting objects within an image by interpreting implicit user instructions, which may encompass subtleties such as contextual cues and open-world knowledge. Despite significant advancements made by existing approaches, they remain constrained by low perceptual resolution, as visual encoders are typically pre-trained at lower resolutions. Furthermore, simply interpolating the positional embeddings of visual encoders to enhance perceptual resolution yields only marginal performance improvements while incurring substantial computational costs. To address this, we propose HRSeg, an efficient model with high-resolution fine-grained perception. It features two key innovations: High-Resolution Perception (HRP) and High-Resolution Enhancement (HRE). The HRP module processes high-resolution images through cropping, integrating local and global features for multi-granularity quality. The HRE module enhances mask features by integrating fine-grained information from high-resolution images, refining their alignment with text features for precise segmentation. Extensive ablation studies validate the effectiveness of our modules, while comprehensive experiments on multiple benchmark datasets demonstrate HRSeg’s superior performance. Code will be available at <https://github.com/Wei HuangLin/HRSeg>.

## CCS Concepts

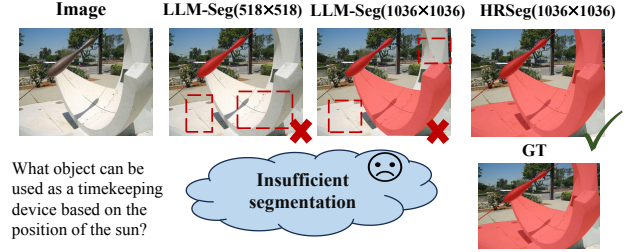
• Computing methodologies → Image segmentation.

## Keywords

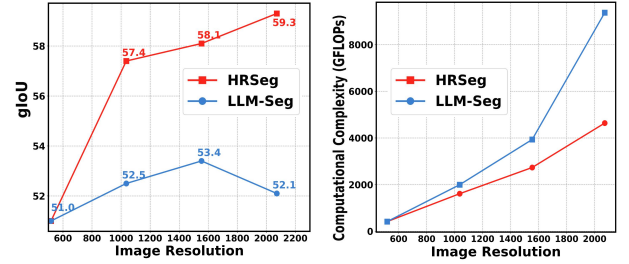
Reasoning Segmentation, Multimodal Large Language Models, High-resolution Perception

## 1 Introduction

Multimodal Large Language Models (MLLMs) [2, 9, 26, 28, 35, 39, 57, 58] have achieved significant advancements in vision-language understanding and reasoning. The reasoning capabilities of these models can be attributed to the exceptional performance of Large



(a) A qualitative comparison between the baseline LLM-Seg and HRSeg



(b) Comparison of Performance and Computational Complexity

Figure 1: (a) Compared to LLM-Seg[56], which misses critical details in this complex scene, HRSeg outperforms it due to its fine-grained perception capabilities. (b) Comparison of performance (gIoU) and computational complexity (GFLOPs) between the two pipelines.

Language Models (LLMs) [14, 22, 33, 48, 54, 65]. Expanding on this, researchers [3, 38, 51, 52, 56, 61–64, 71, 73, 75] are actively investigating methods to leverage reasoning capabilities of MLLMs for referring segmentation [19, 60]. This has given rise to a new task known as *Reasoning Segmentation* [25, 38, 66].

Unlike traditional referring segmentation, reasoning segmentation requires models to interpret implicit instructions to accurately identify specific targets, presenting a significantly more challenging and complex problem. Current research primarily follows two mainstream approaches. The first category is an end-to-end approach, where reasoning and segmentation modules are simultaneously trained on a new dataset. Specifically, this method integrates LLaVA [36] with SAM [24], enabling the model to perform both reasoning and segmentation [25, 63]. This approach typically includes an additional <SEG> token in the LLM’s vocabulary and utilizes its embedding to prompt SAM for segmentation generation. However, fine-tuning pre-trained models such as SAM requires substantial computational resources and may degrade performance due to limited training data availability. To address these challenges,

\*Equal Contribution. †Corresponding Author.

Permission to make digital or hard copies of all or part of this work for personal or classroom use is granted without fee provided that copies are not made or distributed for profit or commercial advantage and that copies bear this notice and the full citation on the first page. Copyrights for components of this work owned by others than ACM must be honored. Abstracting with credit is permitted. To copy otherwise, or republish, to post on servers or to redistribute to lists, requires prior specific permission and/or a fee. Request permissions from [permissions.acm.org](https://permissions.acm.org).

MM '25, Dublin, Ireland

© 2025 ACM.

an alternative approach LLM-Seg [56] employs a two-stage framework that separates reasoning instruction and image segmentation tasks. Initially, SAM is used to generate mask proposals, followed by selecting the correct mask using LLaVA’s reasoning capability. This method relies entirely on the pre-trained SAM for generating mask proposals without fine-tuning, thereby reducing the computational resources required for training while preserving SAM’s robust segmentation capability.

Despite making significant progress, the aforementioned existing works are trained on low-resolution visual encoders, such as DINOv2 [4, 49, 55, 72], which are pre-trained on images at  $518 \times 518$  pixels, and are therefore not inherently capable of processing high-resolution images directly. In light of these observations, our preliminary experiments yielded two important conclusions. **First, high-resolution image features play a crucial role in achieving accurate segmentation results.** As illustrated in the second and fourth images of Fig. 1(a), we observe that the use of low-resolution image inputs can result in inadequate segmentation in scenarios that require fine-grained perception, an issue that our proposed HRSeg, which leverages high-resolution input, effectively addresses. **Second, effectively processing high-resolution image inputs for reasoning segmentation remains a challenging problem.** Specifically, we introduce a naive baseline approach based on LLM-Seg for comparison, where we interpolate the pre-trained positional embeddings within the visual encoder. Although this method supports high-resolution inputs, it still leads to severe under-segmentation in complex scenarios, as evidenced by the comparison of the second and third images in Fig. 1(a). Furthermore, as illustrated on the left side of Fig. 1(b), this approach only improves performance within a specific resolution range; its effectiveness declines significantly as the resolution increases. More importantly, since image encoders typically rely on variants of the Vision Transformer (ViT) [13, 40, 41, 69], their computational complexity increases quadratically with resolution, resulting in significant computational overhead, as shown on the right side of Fig. 1(b).

To address the aforementioned challenges, we introduce an effective and innovative model for high-resolution perception and enhancement in reasoning segmentation tasks, termed High-Resolution Reasoning Segmentation (HRSeg). HRSeg integrates two novel modules to tackle visual perception difficulties in reasoning segmentation tasks. The first module, High-Resolution Perception (HRP), conducts detailed processing of high-resolution image inputs. The high-resolution features produced are then combined with masks generated by SAM to derive mask features through interactive operations. Specifically, the input high-resolution image is cropped according to its aspect ratio and divided into sub-images to align with the pre-trained encoder’s resolution. Region attention is then applied to facilitate the interaction between global image features and cropped local high-resolution features, yielding detailed high-resolution image features. Each mask generated by SAM is processed through a feature aggregation operation, referred to as mask pooling, which aggregates the image features to produce high-quality mask features. The second module, High-Resolution Enhancement (HRE), further enriches the mask features. Since mask features are derived through mask pooling, they lack interaction

with information outside the masked areas in high-resolution images. To address this, the HRE module utilizes high-resolution image features to bolster mask features. This approach enables the mask features to assimilate detailed information from high-resolution images, refining them to improve alignment with text feature <SEG> and enhance segmentation quality.

Based on the HRP and HRE modules, HRSeg emerges as a high-performance, computationally efficient model for the reasoning segmentation task, as shown in Fig. 1(b), where it outperforms the naive baseline in both accuracy and efficiency. Besides, extensive experiments conducted on multiple segmentation benchmark datasets, including ReasonSeg, LLM-Seg40K, and RefCOCO+/g, demonstrate the superior performance of HRSeg. For instance, it achieves a significant improvement of 10% in gIoU and 15.2% in cloU on ReasonSeg compared to the baseline.

In summary, the contributions of this paper are threefold:

- We propose a novel and efficient model, HRSeg, specifically designed to address the challenges of high-resolution image perception and enhancement in the field of reasoning segmentation.
- We introduce two modules, HRP and HRE, to support the fine-grained processing pipeline of HRSeg, enabling the generation of detailed mask features.
- Extensive experiments confirm the exceptional performance of HRSeg in reasoning segmentation task.

## 2 Related Work

### 2.1 Multimodal Large Language Models

With the rapid advancements in Large Language Models (LLMs) [5, 10, 47, 48, 53, 54, 65, 74], their exceptional capabilities have garnered significant attention from researchers. Efforts have been made to extend these capabilities to the vision domain, enabling LLMs to process and understand visual information. This has spurred significant progress in the development of Multimodal Large Language Models (MLLMs) [1, 29, 36, 39, 43, 78]. MLLMs are composed of three primary components: a visual encoder, a visual projector, and an LLM. The visual encoder in MLLMs plays a critical role in extracting and interpreting visual information, with the majority of implementations adopting a Vision Transformer (ViT)-based architecture. However, its capability is constrained by low-resolution inputs, which significantly impede the MLLMs’ ability to capture fine-grained details effectively. To overcome this limitation, several researchers [12, 15, 18, 20, 27, 30, 32, 45, 70] have employed cropping-based methods, which divide the image into multiple patches, enabling the visual encoder to effectively process high-resolution images. The visual projector acts as a crucial intermediary between visual and textual features, facilitating the seamless integration of multimodal information. Prominent implementations of visual projectors include Q-Former [26], Resampler [1], and multilayer perceptrons (MLPs) [36]. Despite the strides made in advancing MLLMs, existing models predominantly focus on image understanding and lack strong capabilities in dense prediction tasks, such as segmentation. To bridge this gap, our research seeks to augment MLLMs by incorporating dense prediction functionalities, thus extending their application from mere image comprehension to tackling reasoning segmentation tasks.

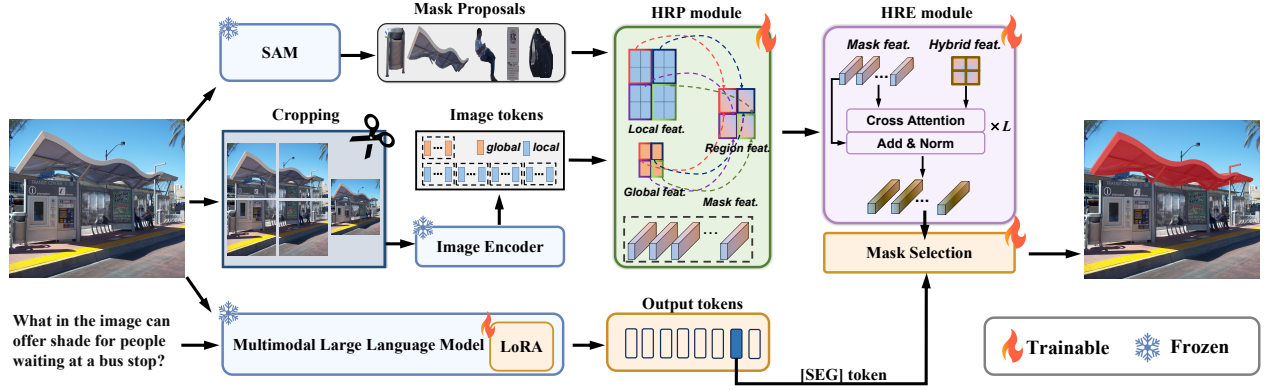


Figure 2: The overview framework of the proposed HRSeg.

## 2.2 Reasoning Segmentation

The reasoning segmentation task involves generating segmentation masks guided by implicit textual instructions, making it a specialized subset of the broader referring segmentation domain. This task was initially introduced by LISA [25]. Current research predominantly follows two main approaches. The first is the end-to-end method, where reasoning and segmentation modules are jointly trained on newly curated datasets. Specifically, LISA integrates LLaVA with SAM by incorporating a  $\langle \text{SEG} \rangle$  token into the LLM’s vocabulary, enabling SAM’s segmentation capabilities to benefit from reasoning. Building upon LISA, PixelLM [52] enhances pixel-level reasoning segmentation by incorporating a segmentation codebook and a lightweight decoder, similar to SAM’s decoder, into an MLLM. In addition, LLaVASeg [67], aiming to preserve the dialog capability of MLLMs, employs chain-of-thought prompting to prompt SAM, without the need to introduce a  $\langle \text{SEG} \rangle$  token. Despite their innovations, these methods face a significant limitation: training the SAM decoder requires substantial computational resources. As an alternative, the two-stage approach employed by LLM-Seg [56] bridges SAM and MLLMs by selecting mask proposals without training the SAM decoder. This method successfully achieves low computational resource consumption while delivering excellent performance. Although each of these methods has its own characteristics, they do not prioritize the capture of fine-grained visual details, which is critical for dense prediction tasks. In other words, they fail to effectively perceive high-resolution images. In light of these insights, we propose the HRSeg model to address the need for high-resolution perception, thereby enhancing the performance of the reasoning segmentation task.

## 3 Method

In this section, we first present a comprehensive overview of the proposed HRSeg framework in Sec. 3.1, highlighting its innovative architecture and key features. Next, we will explore the two main components of the framework: High-Resolution Perception and High-Resolution Enhancement, providing detailed explanations of their intricate functionalities in Sec. 3.2 and Sec. 3.3, respectively. Finally, we present the training objectives of the model in Sec. 3.4.

### 3.1 Overview

Fig. 2 illustrates the complete pipeline of the proposed HRSeg framework. To present the model architecture clearly, we divide it into two main components: *Reasoning* and *Segmentation*.

The **Reasoning component** is primarily handled by the MLLM, which comprises three key elements: a vision encoder to extract features from the image, a large language model to interpret the user’s textual instructions, and a visual projector to align the image and text features seamlessly. Following [25], we adopt the embedding-as-mask paradigm by incorporating the  $\langle \text{SEG} \rangle$  token to the LLM’s vocabulary. Given the input image  $I \in \mathbb{R}^{H \times W \times 3}$  and text instruction  $T$ , we process them through the MLLM to produce the output sequence. The  $\langle \text{SEG} \rangle$  token is activated when a specific target is identified for segmentation. Subsequently, we extract the  $\langle \text{SEG} \rangle$  token embedding and project it into the Mask Selection space:

$$Y_{seg} = f_{MLLM}(I, T), \quad (1)$$

$$\tilde{Y}_{seg} = f_{proj}(Y_{seg}), \quad (2)$$

where the function  $f_{MLLM}(\cdot)$  denotes the processing carried out by MLLM,  $f_{proj}(\cdot)$  denotes the MLP projector and  $Y_{seg}$  corresponds to the embedding of  $\langle \text{SEG} \rangle$  token.

In the **Segmentation part**, the image  $I$  is input to SAM, which generates mask proposals  $\mathbf{M} = \{m_1, m_2, \dots, m_K\} \in \mathbb{R}^{K \times D}$  for the entire image using points prompt arranged in a grid. Note that SAM focuses solely on generating pixel-accurate masks and cannot directly produce mask features. However, downstream segmentation tasks require additional feature extraction. Therefore, our goal is to integrate fine-grained image features with the mask proposals to generate high-quality mask features, enhancing the subsequent matching process.

To leverage the image encoder trained on  $I_v \in \mathbb{R}^{H_v \times W_v \times 3}$ , the image  $I$  is scaled according to its aspect ratio to obtain global view of low-resolution image  $I_g \in \mathbb{R}^{H_g \times W_g \times 3}$  and local view of high-resolution image  $I_l \in \mathbb{R}^{(N \times H_v) \times (N \times W_v) \times 3}$ , where  $N$  represents the magnification. In this manner, the image encoder processes the global and local cropping image to generate corresponding image features:

$$\{\mathbf{F}_g, \mathbf{F}_l\} = f_v(I_g, \text{crop}(I_l)), \quad (3)$$

where  $\mathbf{F}_g \in \mathbb{R}^{N_g \times d}$  and  $\mathbf{F}_l \in \mathbb{R}^{N_l \times d}$  represent the global and local features.  $N_g$  and  $N_l$  denote the number of global and local tokens,

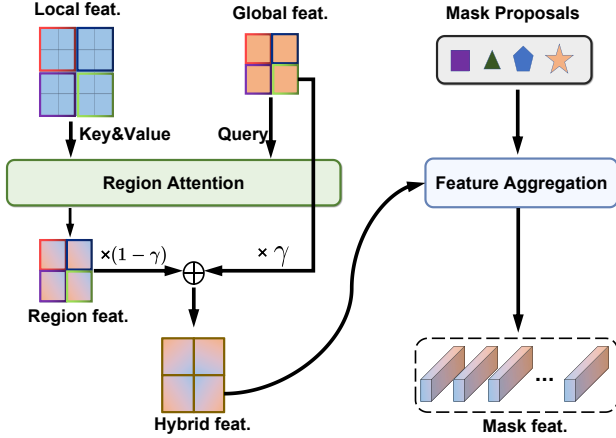


Figure 3: Details of High-Resolution Perception module.

respectively. The function  $f_v(\cdot)$  denotes the image encoder, and  $crop(\cdot)$  refers to using a window  $W \in \mathbb{R}^{H_v \times W_v}$  to crop the image.

Next, the mask proposals  $\mathbf{M}$  and image features  $\{\mathbf{F}_g, \mathbf{F}_l\}$  are fed into the High-Resolution Perception module, enabling the mask proposals to perceive fine-grained hybrid features:

$$\{\mathbf{F}_h, \mathbf{M}_{HRP}\} = f_{HRP}(\mathbf{M}, \mathbf{F}_g, \mathbf{F}_l), \quad (4)$$

where  $\mathbf{F}_h$  denotes the hybrid features, and  $\mathbf{M}_{HRP} \in \mathbb{R}^{K \times d}$  represents the activated mask features. The function  $f_{HRP}(\cdot)$  defines the processing performed by the HRP module, which is elaborated thoroughly in Sec. 3.2.

Subsequently, the mask features  $\mathbf{M}_{HRP}$  are enhanced through HRE module:

$$\mathbf{M}_{HRE} = f_{HRE}(\mathbf{M}_{HRP}, \mathbf{F}_h), \quad (5)$$

where  $\mathbf{M}_{HRE}$  represents the enhanced mask features, and  $f_{HRE}(\cdot)$  defines the enhancement processing, which is explained in Sec. 3.3. The Mask Selection module consists of a fusion module and selection heads, following the approach in [56].

Specifically, the fusion module integrates semantic information from the <SEG> token feature  $\tilde{Y}_{seg}$  with the mask features  $\mathbf{M}_{HRE}$  using self-attention and cross-attention.

The selection heads in the mask selection module consist of two separate MLPs. One maps  $\mathbf{M}_{HRE}$  into the same feature space as the text features, preparing it for the subsequent computation of the similarity score  $S_{sim}$ . The other is used to predict the IoP score  $S_{iop}$ . Firstly, calculate the similarity score  $S_{sim} \in \mathbb{R}^{1 \times K}$  between the mask feature and the token feature:  $S_{sim} = \tilde{Y}_{seg} \times \mathbf{M}_{HRE}^T$ . Next, the mask feature  $\mathbf{M}_{HRE}$  is mapped to the IoP score  $S_{iop}$ . This evaluates the matching degree between each mask proposal and the ground truth mask, making it particularly effective for multi-instance selection. Therefore, based on  $S_{sim}$  and  $S_{iop}$ , we develop different strategies for mask selection. Further details are provided in the Experiments section.

$$\mathbf{M}_{sel} = f_{sel}(\mathbf{M}_{HRE}, \tilde{Y}_{seg}), \quad (6)$$

where the function  $f_{sel}(\cdot)$  refers to the processing that combines Reasoning and Segmentation components.

### 3.2 High-Resolution Perception

Given the two types of image features,  $\mathbf{F}_g$  and  $\mathbf{F}_l$ , the High-Resolution Perception module first enhances the global view of the image by integrating local detail features. Then, the enriched hybrid features,  $\mathbf{F}_h$ , are utilized to allow the mask region proposals  $\mathbf{M}$  to perceive and leverage them effectively. This process is vividly illustrated in Fig. 3.

Firstly, we reshape  $\mathbf{F}_g$  and  $\mathbf{F}_l$  to get  $\mathbf{F}_g \in \mathbb{R}^{n_g \times n_g \times d}$  and  $\mathbf{F}_l \in \mathbb{R}^{n_l \times n_l \times d}$ , where  $N_g = n_g \times n_g$ ,  $N_l = n_l \times n_l$ , and  $n_l = N \times n_g$ . To perform region-level attention, we provide a definition to capture the region of  $\mathbf{F}_l$ :

$$R(\mathbf{F}_l) = \mathbf{F}_l[i : i + N, j : j + N, :], 0 \leq i, j \leq n_l - N, \quad (7)$$

where  $R(\mathbf{F}_l) \in \mathbb{R}^{(n_g \times n_g) \times (N \times N) \times d}$  represents the region features.

Next, we use  $\mathbf{F}_g \in \mathbb{R}^{(n_g \times n_g) \times 1 \times d}$  as the query feature to compute the attention map between each query and the corresponding region features, enabling to identify the relevant detail region features for the query. The query feature then absorbs the high-resolution features by performing a weighted sum of the region features based on the attention maps. The region attention is formulated as follows:

$$\mathbf{F}_r = \text{Softmax}\left(\frac{(\mathbf{F}_g \mathbf{W}_g^q)(R(\mathbf{F}_l) \mathbf{W}_l^k)^T}{\sqrt{d}}\right)(R(\mathbf{F}_l) \mathbf{W}_l^v), \quad (8)$$

where  $\mathbf{W}_g^q, \mathbf{W}_l^k, \mathbf{W}_l^v \in \mathbb{R}^{d \times d}$  are the trainable parameters of the projection layers.  $\mathbf{F}_r \in \mathbb{R}^{(n_g \times n_g) \times d}$  denotes the region features.

To preserve the global perspective of the image features, we perform a pixel-wise addition of  $\mathbf{F}_r$  and  $\mathbf{F}_g$ . This fusion yields hybrid features  $\mathbf{F}_h$  that seamlessly integrate the fine-grained information from  $\mathbf{F}_r$  with the holistic perspective provided by  $\mathbf{F}_g$ , thereby enriching the feature representation:

$$\mathbf{F}_h = \gamma \times \mathbf{F}_g + (1 - \gamma) \times \mathbf{F}_r, \quad (9)$$

where  $\gamma$  represents the weight assigned to different features.

Finally, we enable the mask proposals to perceive fine-grained hybrid features. The feature aggregation process can be formulated as follows:

$$\mathbf{M}_{HRP} = \frac{\mathbf{M} \cdot \mathbf{F}_r^T}{\sum \mathbf{M}}, \quad (10)$$

where  $\mathbf{M}_{HRP} \in \mathbb{R}^{K \times d}$  denotes the activated mask feature.

### 3.3 High-Resolution Enhancement

In Sec. 3.2, we introduced the process of enabling mask proposals to perceive high-resolution features within their internal regions. To further enhance the representation of each mask, it is essential not only to consider its own features but also to integrate the global features of the entire image. Specifically, we achieve this by leveraging the hybrid feature  $\mathbf{F}_h$ , a fine-grained representation that incorporates high-resolution information, to enhance the mask feature  $\mathbf{M}_{HRP}$ .

Specifically, to incorporate the global information of the hybrid feature into the mask features, we employ a cross-attention mechanism between them. Additionally, a residual mechanism is utilized to preserve the original mask features. The above operations are

stacked for  $L$  layers. This interaction can be mathematically formulated as follows:

$$\mathbf{M}_{HRE} = \text{Softmax}\left(\frac{(\mathbf{M}_{HRP}\mathbf{W}_m^q)(\mathbf{F}_h\mathbf{W}_h^k)^\top}{\sqrt{d}}\right)(\mathbf{F}_h\mathbf{W}_h^v), \quad (11)$$

$$\mathbf{M}_{HRE} = \text{Norm}(\mathbf{M}_{HRP} + \mathbf{M}_{HRE}), \quad (12)$$

where  $\mathbf{W}_m^q, \mathbf{W}_h^k, \mathbf{W}_h^v \in \mathbb{R}^{d \times d}$  are the trainable parameters of the projection layers. The function  $\text{Norm}(\cdot)$  represents layer normalization.

Therefore, the mask feature set  $\mathbf{M}_{HRE}$  contains not only fine-grained object-level information but also high-resolution features integrated throughout the image.

### 3.4 Training Objectives

The proposed model is trained using both mask selection loss  $\mathcal{L}_{sel}$  and text generation loss  $\mathcal{L}_{text}$ .

Specifically,  $\mathcal{L}_{sel}$  consists of two components: one focuses on matching the similarity and IoU distributions to select the mask that best aligns with the text, while the other component is used to supplement the mask, enabling the selection of multiple masks that better match the text under a certain threshold. This can be formally expressed as:

$$\mathcal{L}_{sel} = \lambda_{sim}\mathcal{L}_{sim} + \lambda_{sup}\mathcal{L}_{sup}, \quad (13)$$

$$\mathcal{L}_{sim} = \text{KL}\left(S_{sim}, \text{IoU}(\mathbf{M}_{HRE}, \mathbf{M}_{gt})\right), \quad (14)$$

$$\mathcal{L}_{sup} = \text{MSE}(\text{IoP}_{pred} - \text{IoP}_{gt}), \quad (15)$$

where  $\mathbf{M}_{gt} \in \mathbb{R}^{1 \times d}$  represents the ground-truth mask of the image. The function  $\text{IoU}(\cdot)$  calculates the Intersection over Union (IoU) between  $\mathbf{M}_{HRE}$  and  $\mathbf{M}_{gt}$ , and  $\text{KL}(\cdot)$  represents the KL divergence used to measure the two distributions. In addition, the IoP is the ratio of the area of the intersection between the ground truth and the mask proposal to the area of the proposal.

The text loss  $\mathcal{L}_{text}$  is the auto-regressive cross-entropy loss used for text generation. Thus, the model's final loss can be expressed as:

$$\mathcal{L} = \lambda_{text}\mathcal{L}_{text} + \lambda_{sel}\mathcal{L}_{sel}. \quad (16)$$

## 4 Experiments

### 4.1 Dataset and Evaluation Metric

Following [25], we train HRSeg using multiple datasets from different tasks. The first category includes semantic segmentation datasets, such as COCO-Stuff [6], ADE20K [76], PACO-LVIS [50], PartImageNet [17], and PASCAL-Part [7]. The second category includes referring segmentation datasets, namely Refc1ef, RefCOCO, RefCOCO+ [23], and RefCOCOG [46]. The final category comprises reasoning segmentation datasets, including ReasonSeg [25] and LLM-Seg40K [56].

We evaluate our method using two metrics: gIoU, which computes the average IoU over all samples, and cIoU, which calculates the cumulative intersection over the cumulative union. While both metrics are used for comparison with state-of-the-art methods in our experiments, prior studies [25, 56] have shown that cIoU is heavily influenced by large objects. Therefore, we focus on gIoU for a more balanced evaluation.

### 4.2 Implementation Details

We trained HRSeg for one day on 2 NVIDIA 3090 GPUs using the DeepSpeed engine. The mask proposals are generated using a  $32 \times 32$  grid of points to prompt SAM. The default MLLM is LLaVA-7B-v1-1, with LoRA applied for efficient fine-tuning. The image encoder used for the HRP module is DINOv2-ViT-L [49], which is pretrained on images of size  $518 \times 518$  pixels. We use AdamW [42] as the optimizer and apply WarmupDecayLR to adjust the learning rate. The initial learning rate is set to 0.0003. We use a batch size of 2 per GPU, with a gradient accumulation step of 10. For high-resolution images, we set  $N = 2$  by default, which corresponds to an image size of  $518 \times 2 = 1036$ . The  $\gamma$  in the HRP module is set to 0.8 to weight the features, and the  $L$  value is set to 2 in the HRE module. For the loss function, the weights for the text loss ( $\lambda_{text}$ ) and selection loss ( $\lambda_{sel}$ ) are both set to 1.0.

### 4.3 Results on ReasonSeg

Table 1 provides a detailed comparison of our proposed HRSeg against various state-of-the-art segmentation models. Notably, HRSeg is a novel model tailored for high-resolution reasoning segmentation tasks.

The experimental results reveal that HRSeg consistently outperforms prior methods across all metrics and evaluation splits on the ReasonSeg dataset. Without fine-tuning, HRSeg achieves remarkable gains in gIoU and cIoU, outperforming LLM-Seg by 2.7% and 8.8% on the validation set, and by 6.4% and 9.2% on the overall test set, respectively. Furthermore, HRSeg demonstrates superior handling of both short and long queries, achieving a substantial 5.6% and 11.0% improvement in gIoU and cIoU over LLM-Seg for short queries, and a 6.6% and 9.9% improvement for long queries. Fine-tuning on the ReasonSeg training split further boosts the performance of HRSeg, achieving superior results across all evaluation metrics.

The experiments also reveal that in long-query instructions, which are more complex and require richer visual details, HRSeg outperforms LLM-Seg by 6.6%. This improvement is 4.3% higher than that observed in short-query scenarios. **This demonstrates that HRSeg excels at capturing fine-grained visual features, allowing it to generate high-quality mask features and achieve better alignment with complex queries.**

Therefore, we attribute our model's superior performance to its ability to leverage high-resolution visual information, which not only enhances the level of detail in the segmentation but also facilitates the handling of implicit query text, thereby improving overall segmentation accuracy.

### 4.4 Results on LLM-Seg40K

The LLM-Seg40K [56] is an additional supplement to the reasoning segmentation dataset. It is derived from LVIS [16] and EgoObjects [77], and includes both high-quality photographic images and egocentric images.

We follow the same setting as LLM-Seg and conduct evaluation on this dataset. The results in Table 2 demonstrate the significant performance advantages of HRSeg over prior methods on the LLM-Seg40K dataset. Without fine-tuning, HRSeg achieves significant improvements over LLM-Seg, with gains of 8.3% in gIoU and 5.0%



**Table 1: The performance of various methods on the ReasonSeg dataset. "ft" indicates whether the method has been fine-tuned using the training split of the ReasonSeg dataset.**

Method	val		test					
	overall		short query		long query		overall	
	gIoU	cIoU	gIoU	cIoU	gIoU	cIoU	gIoU	cIoU
OVSeg [31]	28.5	18.6	18.0	15.5	28.7	22.5	26.1	20.8
GRES [34]	22.4	19.9	17.6	15.0	22.6	23.8	21.3	22.0
X-Decoder [79]	22.6	17.9	20.4	11.6	22.2	17.5	21.7	16.3
SEEM [80]	25.5	21.2	20.1	11.5	25.6	20.8	24.3	18.7
Grounded-SAM [37]	26.0	14.5	17.8	10.8	22.4	18.6	21.3	16.4
LISA [25]	44.4	46.0	37.6	34.4	36.6	34.7	36.8	34.1
LLM-Seg [56]	47.4	35.4	39.8	32.9	41.3	33.8	40.2	33.4
SAM4MLLM [8]	46.7	48.1	-	-	-	-	-	-
HRSeg	50.1	47.1	42.1	37.7	47.9	43.7	46.6	42.6
HRSeg-LLaVA-v1.6	<b>56.7</b>	<b>55.4</b>	<b>47.9</b>	<b>44.2</b>	<b>56.6</b>	<b>53.2</b>	<b>54.6</b>	<b>51.2</b>
LISA (ft)	51.0	50.6	40.6	40.6	49.4	51.0	47.3	48.4
LLM-Seg (ft)	52.3	47.5	41.1	40.2	49.8	49.1	47.9	46.2
HRSeg (ft)	57.4	54.7	43.4	41.7	54.4	54.5	51.6	50.5
HRSeg-LLaVA-v1.6 (ft)	<b>64.9</b>	<b>63.1</b>	<b>49.5</b>	<b>48.7</b>	<b>59.2</b>	<b>58.9</b>	<b>57.0</b>	<b>57.2</b>

**Table 2: Performance comparison between HRSeg and prior works on the validation split of the LLM-Seg40K dataset.**

Method	gIoU	cIoU
GRES	14.2	15.9
LISA	33.2	37.9
LLM-Seg	36.0	39.4
HRSeg	<b>44.3</b>	<b>44.4</b>
LISA (ft)	37.6	48.5
LLM-Seg (ft)	45.5	54.2
HRSeg (ft)	<b>58.7</b>	<b>58.0</b>

in cIoU respectively. Fine-tuning further enhances HRSeg’s performance, establishing new state-of-the-art results on LLM-Seg40K. Specifically, HRSeg achieves a remarkable 58.7 gIoU and 58.0 cIoU, outperforming fine-tuned LLM-Seg by 13.2% in gIoU and 3.8% in cIoU. These results highlight HRSeg’s robust ability to leverage fine-grained visual information, effectively addressing the diverse visual challenges presented by the high-quality photographic and egocentric images in the dataset.

#### 4.5 Results on Referring Segmentation

Referring segmentation differs from reasoning segmentation in its use of a definite query. Table 3 presents the comparison results on referring segmentation datasets. Our model demonstrates competitive performance compared to recent SOTA methods, indicating its capability to effectively handle referring segmentation tasks. Furthermore, replacing MLLM with the more powerful LLaVA 1.6 leads to a notable improvement in performance.

#### 4.6 Ablation Study

**Study on HRP and HRE.** To assess the effectiveness of our proposed HRP and HRE modules, we performed ablation studies by integrating each module into the baseline model. Table 4 presents the results of the ablation study, highlighting the contributions of the HRP and HRE modules to performance improvements. The

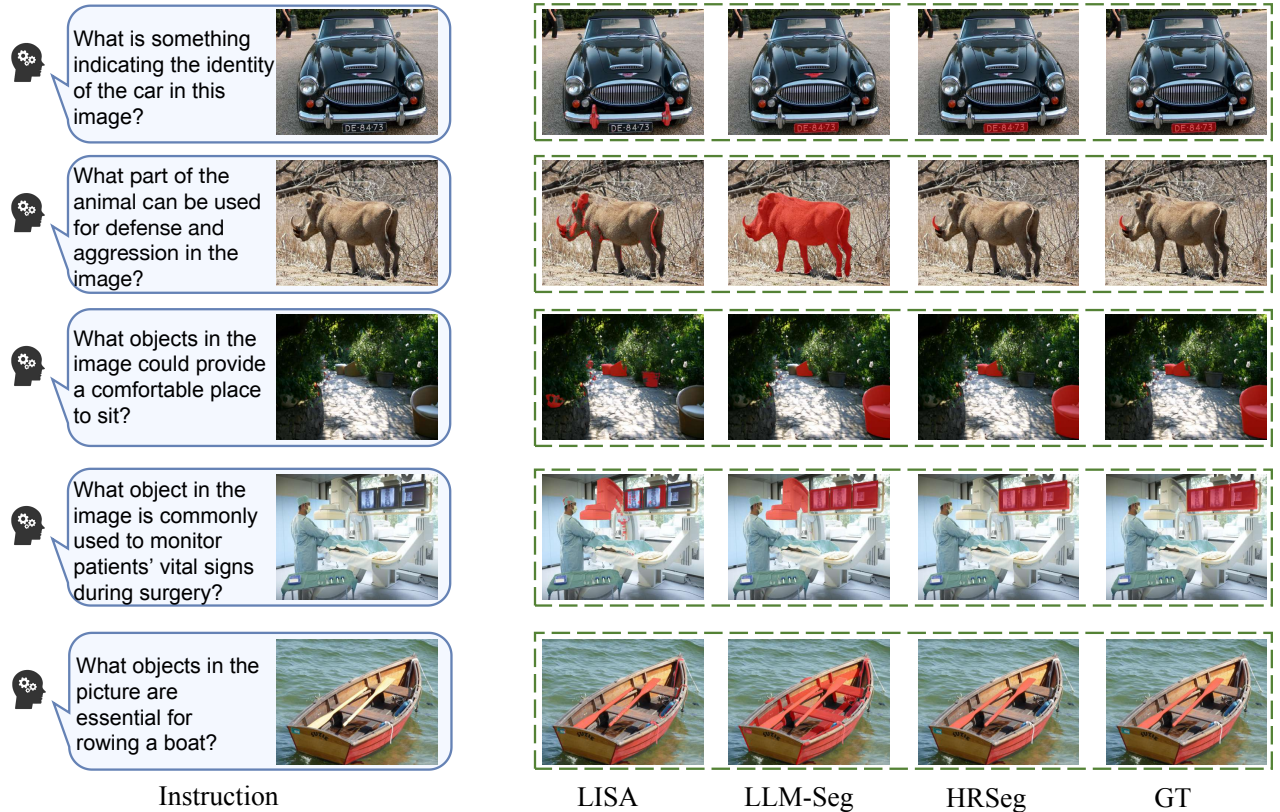
integration of the HRP module into the baseline yields significant improvements, with gIoU and cIoU metrics on the ReasonSeg validation set increasing from 52.3 to 55.2 and 47.5 to 52.1, respectively. Similarly, on the LLM-Seg40K validation set, gIoU improves from 45.5 to 53.7, and cIoU rises from 54.2 to 55.6. Adding the HRE module alongside HRP further enhances performance, showcasing their complementary effects. The combined HRP and HRE modules achieve the highest metrics, with a gIoU of 57.4 and cIoU of 54.7 on the ReasonSeg validation set. These results underscore the HRP module’s strength in high-resolution feature perception and the HRE module’s role in refining these features, collectively driving state-of-the-art segmentation performance.

**Study on the weight  $\gamma$ .** To evaluate the weight allocation when combining global features and region features, we analyze the impact of varying the value of  $\gamma$  within the HRP module. As shown in Table 5, the results demonstrate that the choice of  $\gamma$  significantly influences the model’s ability to capture hybrid information from these two types of features. When  $\gamma$  is too low, the contribution of global features is diminished, limiting the model’s holistic understanding of the scene. Conversely, overly high values of  $\gamma$  reduce the impact of region-specific details, which are crucial for precise reasoning segmentation. The optimal setting,  $\gamma = 0.8$ , achieves the best balance, effectively leveraging both global context and detailed regional information to enhance the model’s reasoning capability.

**Study on the image resolution.** To further investigate the impact of increased image resolution on the performance of our model, we conducted an ablation study on image resolution. As shown in Table 6,  $N$  represents the magnification factor of the pre-trained encoder resolution. The results indicate that increasing the resolution of the input images enhances the model’s ability to capture finer details, which leads to better segmentation performance. Specifically, higher resolution allows the model to preserve more granular information, thus improving both global and local reasoning. However, this performance gain gradually diminishes as the resolution increases. While performance continues to improve with higher

**Table 3: Comparison of referring segmentation results (cIoU) between HRSeg (ours) and existing methods.**

Method	refCOCO			refCOCO+			refCOCOg	
	val	testA	testB	val	testA	testB	val(U)	test(U)
<i>traditional methods</i>								
MCN [44]	62.4	64.2	59.7	50.6	55.0	44.7	49.2	49.4
VL [11]	67.5	70.5	65.2	56.3	61.0	50.1	55.0	57.7
CRIS [60]	70.5	73.2	66.1	62.3	68.1	53.7	59.9	60.4
LAVT [68]	72.7	75.8	68.8	62.1	68.4	55.1	61.2	62.1
ReLA [34]	73.8	76.5	70.2	66.0	71.0	57.7	65.0	66.0
SEEM [80]	-	-	-	-	-	-	65.7	-
<i>LLM based</i>								
LISA-LLaVA-v1 [25]	74.9	79.1	72.3	65.1	70.8	58.1	67.9	70.6
PixelLM-LLaVA-v1 [52]	73.0	76.5	68.2	66.3	71.7	58.3	69.3	70.5
LLaVASeg-LLaVA-v1 [67]	76.2	79.1	72.9	65.7	71.4	57.7	69.8	70.1
GSVA-LLaVA-v1 [63]	76.4	77.4	72.8	64.5	67.7	58.6	71.1	72.0
M <sup>2</sup> SA-LLaVA-v1 [21]	74.0	76.8	69.7	63.1	67.2	56.1	67.0	68.3
GLaMM-LLaVA-v1.5 [51]	79.5	83.2	76.9	72.6	78.7	64.6	74.2	74.9
SAM4MLLM-LLaVA-v1.6 [8]	79.6	82.8	76.1	73.5	77.8	65.8	74.5	75.6
SegLLM-LLaVA-v1.5 [59]	80.2	81.5	75.4	70.3	73.0	62.5	72.6	73.6
HRSeg-LLaVA-v1	77.1	79.7	73.2	66.4	72.4	58.9	71.4	72.8
HRSeg-LLaVA-v1.6	<b>81.2</b>	<b>83.4</b>	<b>78.1</b>	<b>73.7</b>	<b>79.1</b>	<b>67.1</b>	<b>75.6</b>	<b>76.4</b>

**Figure 4: Qualitative results comparison between HRSeg (Ours) and other methods. HRSeg showcases its fine-grained perception capabilities, delivering exceptional segmentation performance.**

**Table 4: Ablation study on the core components of HRSeg.** HRP and HRE denote the proposed High-Resolution Perception and High-Resolution Enhancement module.

HRP	HRE	ReasonSeg val		LLM-Seg40k val	
		gIoU	cIoU	gIoU	cIoU
		52.3	47.5	45.5	54.2
✓		55.2↑ 5.5%	52.1↑ 9.7%	53.7↑ 18.0%	55.6↑ 2.6%
✓	✓	<b>57.4↑ 10.0%</b>	<b>54.7↑ 15.2%</b>	<b>58.7↑ 29.0%</b>	<b>58.0↑ 7.0%</b>

**Table 5: Ablation study on the weight  $\gamma$  in the HRP module.**

$\gamma$	ReasonSeg val	
	gIoU	cIoU
0.5	56.3	53.9
0.6	56.5	54.1
0.7	57.1	54.3
0.8	<b>57.4</b>	<b>54.7</b>
0.9	56.9	54.4

**Table 6: Ablation study on the size of high-resolution images.**

N	ReasonSeg val		LLM-Seg40k val	
	gIoU	cIoU	gIoU	cIoU
-	52.3	47.5	45.5	54.2
2	57.4	54.7	58.7	58.0
3	58.1	54.5	61.2	57.3
4	59.3	55.3	62.1	58.2

values of  $N$ , the computational cost associated with larger image sizes becomes significantly higher, leading to increased memory usage and processing time. Thus,  $N = 2$  was chosen as the optimal resolution for our model, as the marginal gains beyond this point are not substantial enough to justify the higher resource demands.

**Study on the mask selection strategy.** To investigate the impact of mask selection strategies on final segmentation performance, we experimented with different strategies. As shown in Table 7, we first attempted to select a single mask as the final segmentation result by choosing the mask with the highest  $S_{sim}$  or  $S_{IOP}$  score. Experimental results show that this single-mask selection strategy performs significantly worse than the multi-mask selection strategy. Therefore, among the five strategies, we choose one that considers masks with high semantic similarity to the text features while also selecting as many masks as possible with high  $S_{IOP}$  scores. This strategy achieved gIoU of 56.9 and cIoU of 54.4 on the ReasonSeg validation set. By adopting this selection strategy, HRSeg effectively combines multiple over-segmented proposals from SAM, leading to optimal performance. A qualitative analysis of this strategy can be found in the supplementary materials. It demonstrates how our strategy works in complex scenarios, and compared to other models, the final segmentation performance is notably improved due to the high-resolution perception technique introduced by HRSeg.

Furthermore, we conducted experiments on the threshold of  $S_{IOP}$ . As shown in Table 8, the initial threshold of 0.5 did not yield the best performance. Instead, the optimal performance was achieved when the threshold was set to 0.7. This suggests that the initial setting

**Table 7: Ablation study on the mask selection strategy.** In Multi-mask selection strategy, the threshold is 0.5 and  $K$  is 10.

Mask selection strategy	ReasonSeg val	
	gIoU	cIoU
Single-mask selection strategy		
Top1 $S_{sim}$	52.4	51.9
Top1 $S_{IOP}$	51.9	50.8
Multi-mask selection strategy		
$S_{IOP}$ from threshold	55.1	52.6
Top K $S_{sim}$	54.2	53.1
Top K $S_{sim} \cap S_{IOP}$ from threshold	<b>56.9</b>	<b>54.4</b>

**Table 8: Ablation study on the threshold of  $S_{IOP}$** 

threshold	ReasonSeg val	
	gIoU	cIoU
0.5	56.9	54.4
0.6	57.1	54.5
<b>0.7</b>	<b>57.4</b>	<b>54.7</b>
0.8	56.7	54.2
0.9	55.9	53.8

included some low-confidence masks, which negatively impacted segmentation performance.

## 4.7 Qualitative Results

Fig. 4 presents visualization examples from the ReasonSeg dataset, comparing HRSeg with other SOTA methods. It is evident that HRSeg consistently delivers more accurate and detailed segmentation results. As shown in the first three rows of the figure, HRSeg performs exceptionally well in scenarios involving small objects or situations that require more detailed visual perception. We attribute this to the key components of HRSeg, which enhance its ability to perceive fine-grained visual details, enabling it to interpret implicit instructions and achieve precise segmentation. In contrast, other methods often produce incorrect or imprecise segmentation results in complex scenarios. More visualization results, including analyses of how the model perceives fine-grained details and its failure cases, can be found in the supplementary materials.

## 5 Conclusion

In this paper, we introduce HRSeg, an advanced framework specifically designed to capture fine-grained visual details and address the challenges of high-resolution reasoning segmentation tasks. Through comprehensive experimental evaluations, we demonstrate that the proposed HRP and HRE modules enhance segmentation performance across various benchmark datasets. These results underscore the effectiveness and adaptability of our framework, establishing it as a robust solution for tackling complex real-world segmentation scenarios. We hope HRSeg will serve as a strong foundation for future innovations in reasoning segmentation task.



## References

- [1] Jinze Bai, Shuai Bai, Shusheng Yang, Shijie Wang, Sinan Tan, Peng Wang, Junyang Lin, Chang Zhou, and Jingren Zhou. 2023. Qwen-vl: A frontier large vision-language model with versatile abilities. *arXiv preprint arXiv:2308.12966* (2023).
- [2] Shuai Bai, Keqin Chen, Xuejing Liu, Jialin Wang, Wenbin Ge, Sibao Song, Kai Dang, Peng Wang, Shijie Wang, Jun Tang, et al. 2025. Qwen2. 5-vl technical report. *arXiv preprint arXiv:2502.13923* (2025).
- [3] Zechen Bai, Tong He, Haiyang Mei, Pichao Wang, Ziteng Gao, Joya Chen, Zheng Zhang, and Mike Zheng Shou. 2024. One token to seg them all: Language instructed reasoning segmentation in videos. *Advances in Neural Information Processing Systems* 37 (2024), 6833–6859.
- [4] Fan Bao, Shen Nie, Kaiwen Xue, Yue Cao, Chongxuan Li, Hang Su, and Jun Zhu. 2023. All are worth words: A vit backbone for diffusion models. In *Proceedings of the IEEE/CVF conference on computer vision and pattern recognition*. 22669–22679.
- [5] Xiao Bi, Deli Chen, Guanting Chen, Shanhuang Chen, Damai Dai, Chengqi Deng, Honghui Ding, Kai Dong, Qiusi Du, Zhe Fu, et al. 2024. Deepseek llm: Scaling open-source language models with longtermism. *arXiv preprint arXiv:2401.02954* (2024).
- [6] Holger Caesar, Jasper Uijlings, and Vittorio Ferrari. 2018. Coco-stuff: Thing and stuff classes in context. In *Proceedings of the IEEE conference on computer vision and pattern recognition*. 1209–1218.
- [7] Xianjie Chen, Roozbeh Mottaghi, Xiaobai Liu, Sanja Fidler, Raquel Urtasun, and Alan Yuille. 2014. Detect what you can: Detecting and representing objects using holistic models and body parts. In *Proceedings of the IEEE conference on computer vision and pattern recognition*. 1971–1978.
- [8] Yi-Chia Chen, Wei-Hua Li, Cheng Sun, Yu-Chiang Frank Wang, and Chu-Song Chen. 2024. SAM4MLLM: Enhance Multi-Modal Large Language Model for Referring Expression Segmentation. In *European Conference on Computer Vision*. Springer, 323–340.
- [9] Zhe Chen, Jiannan Wu, Wenhai Wang, Weijie Su, Guo Chen, Sen Xing, Muyan Zhong, Qinglong Zhang, Xizhou Zhu, Lewei Lu, et al. 2024. Internvl: Scaling up vision foundation models and aligning for generic visual-linguistic tasks. In *Proceedings of the IEEE/CVF conference on computer vision and pattern recognition*. 24185–24198.
- [10] Wei-Lin Chiang, Zhuohan Li, Zi Lin, Ying Sheng, Zhanghao Wu, Hao Zhang, Lianmin Zheng, Siyuan Zhuang, Yonghao Zhuang, Joseph E Gonzalez, et al. 2023. Vicuna: An open-source chatbot impressing gpt-4 with 90% chatgpt quality. See <https://vicuna.lmsys.org> (accessed 14 April 2023) 2, 3 (2023), 6.
- [11] Henghui Ding, Chang Liu, Suchen Wang, and Xudong Jiang. 2021. Vision-language transformer and query generation for referring segmentation. In *Proceedings of the IEEE/CVF International Conference on Computer Vision*. 16321–16330.
- [12] Xiaoyi Dong, Pan Zhang, Yuhang Zang, Yuhang Cao, Bin Wang, Linke Ouyang, Songyang Zhang, Haodong Duan, Wenwei Zhang, Yining Li, et al. 2024. Internlm-xcomposer2-4khd: A pioneering large vision-language model handling resolutions from 336 pixels to 4k hd. *arXiv preprint arXiv:2404.06512* (2024).
- [13] Alexey Dosovitskiy. 2020. An image is worth 16x16 words: Transformers for image recognition at scale. *arXiv preprint arXiv:2010.11929* (2020).
- [14] Daya Guo, Dejian Yang, Haowei Zhang, Junxiao Song, Ruoyu Zhang, Runxin Xu, Qihao Zhu, Shirong Ma, Peiyi Wang, Xiao Bi, et al. 2025. Deepseek-r1: Incentivizing reasoning capability in llms via reinforcement learning. *arXiv preprint arXiv:2501.12948* (2025).
- [15] Zonghao Guo, Ruyi Xu, Yuan Yao, Junbo Cui, Zanlin Ni, Chunjiang Ge, Tat-Seng Chua, Zhiyuan Liu, and Gao Huang. 2025. Llava-uhd: an lmm perceiving any aspect ratio and high-resolution images. In *European Conference on Computer Vision*. Springer, 390–406.
- [16] Agrim Gupta, Piotr Dollar, and Ross Girshick. 2019. Lvis: A dataset for large vocabulary instance segmentation. In *Proceedings of the IEEE/CVF conference on computer vision and pattern recognition*. 5356–5364.
- [17] Ju He, Shuo Yang, Shaokang Yang, Adam Kortylewski, Xiaodong Yuan, Jie-Neng Chen, Shuai Liu, Cheng Yang, Qihang Yu, and Alan Yuille. 2022. Partimagenet: A large, high-quality dataset of parts. In *European Conference on Computer Vision*. Springer, 128–145.
- [18] Anwen Hu, Haiyang Xu, Jiabo Ye, Ming Yan, Liang Zhang, Bo Zhang, Chen Li, Ji Zhang, Qin Jin, Fei Huang, et al. 2024. mplug-docowl 1.5: Unified structure learning for ocr-free document understanding. *arXiv preprint arXiv:2403.12895* (2024).
- [19] Ronghang Hu, Marcus Rohrbach, and Trevor Darrell. 2016. Segmentation from natural language expressions. In *Computer Vision—ECCV 2016: 14th European Conference, Amsterdam, The Netherlands, October 11–14, 2016, Proceedings, Part I* 14. Springer, 108–124.
- [20] Mingxin Huang, Yuliang Liu, Dingkan Liang, Lianwen Jin, and Xiang Bai. 2024. Mini-monkey: Alleviating the semantic sawtooth effect for lightweight mllms via complementary image pyramid. *arXiv preprint arXiv:2408.02034* (2024).
- [21] Donggon Jang, Yucheo Cho, Suin Lee, Taehyeon Kim, and Dae-Shik Kim. 2025. MMR: A Large-scale Benchmark Dataset for Multi-target and Multi-granularity Reasoning Segmentation. *arXiv preprint arXiv:2503.13881* (2025).
- [22] Albert Q Jiang, Alexandre Sablayrolles, Antoine Roux, Arthur Mensch, Blanche Savary, Chris Bamford, Devendra Singh Chaplot, Diego de las Casas, Emma Bou Hanna, Florian Bressand, et al. 2024. Mixtral of experts. *arXiv preprint arXiv:2401.04088* (2024).
- [23] Sahar Kazemzadeh, Vicente Ordonez, Mark Matten, and Tamara Berg. 2014. Referitgame: Referring to objects in photographs of natural scenes. In *Proceedings of the 2014 conference on empirical methods in natural language processing (EMNLP)*. 787–798.
- [24] Alexander Kirillov, Eric Mintun, Nikhila Ravi, Hanzi Mao, Chloe Rolland, Laura Gustafson, Tete Xiao, Spencer Whitehead, Alexander C Berg, Wan-Yen Lo, et al. 2023. Segment anything. In *Proceedings of the IEEE/CVF International Conference on Computer Vision*. 4015–4026.
- [25] Xin Lai, Zhuotao Tian, Yukang Chen, Yanwei Li, Yuhui Yuan, Shu Liu, and Jiaya Jia. 2024. Lisa: Reasoning segmentation via large language model. In *Proceedings of the IEEE/CVF Conference on Computer Vision and Pattern Recognition*. 9579–9589.
- [26] Junnan Li, Dongxu Li, Silvio Savarese, and Steven Hoi. 2023. Blip-2: Bootstrapping language-image pre-training with frozen image encoders and large language models. In *International conference on machine learning*. PMLR, 19730–19742.
- [27] Wentong Li, Yuqian Yuan, Jian Liu, Dongqi Tang, Song Wang, Jie Qin, Jianke Zhu, and Lei Zhang. 2024. Tokenpacker: Efficient visual projector for multimodal llm. *arXiv preprint arXiv:2407.02392* (2024).
- [28] Xiangtai Li, Haobo Yuan, Wei Li, Henghui Ding, Size Wu, Wenwei Zhang, Yining Li, Kai Chen, and Chen Change Loy. 2024. Omg-seg: Is one model good enough for all segmentation?. In *Proceedings of the IEEE/CVF conference on computer vision and pattern recognition*. 27948–27959.
- [29] Yanwei Li, Yuechen Zhang, Chengyao Wang, Zhisheng Zhong, Yixin Chen, Ruihang Chu, Shaoteng Liu, and Jiaya Jia. 2024. Mini-gemini: Mining the potential of multi-modality vision language models. *arXiv preprint arXiv:2403.18814* (2024).
- [30] Zhang Li, Biao Yang, Qiang Liu, Zhiyi Ma, Shuo Zhang, Jingxu Yang, Yabo Sun, Yuliang Liu, and Xiang Bai. 2024. Monkey: Image resolution and text label are important things for large multi-modal models. In *Proceedings of the IEEE/CVF Conference on Computer Vision and Pattern Recognition*. 26763–26773.
- [31] Feng Liang, Bichen Wu, Xiaoliang Dai, Kumpeng Li, Yinan Zhao, Hang Zhang, Peizhao Zhang, Peter Vajda, and Diana Marculescu. 2023. Open-vocabulary semantic segmentation with mask-adapted clip. In *Proceedings of the IEEE/CVF Conference on Computer Vision and Pattern Recognition*. 7061–7070.
- [32] Ziyi Lin, Chris Liu, Renrui Zhang, Peng Gao, Longtian Qiu, Han Xiao, Han Qiu, Chen Lin, Wenqi Shao, Keqin Chen, et al. 2023. Sphinx: The joint mixing of weights, tasks, and visual embeddings for multi-modal large language models. *arXiv preprint arXiv:2311.07575* (2023).
- [33] Aixiu Liu, Bei Feng, Bing Xue, Bingxuan Wang, Bochao Wu, Chengda Lu, Cheng-gang Zhao, Chengqi Deng, Chenyu Zhang, Chong Ruan, et al. 2024. Deepseek-v3 technical report. *arXiv preprint arXiv:2412.19437* (2024).
- [34] Chang Liu, Henghui Ding, and Xudong Jiang. 2023. Gres: Generalized referring expression segmentation. In *Proceedings of the IEEE/CVF conference on computer vision and pattern recognition*. 23592–23601.
- [35] Haotian Liu, Chunyuan Li, Yuheng Li, Bo Li, Yunnan Zhang, Sheng Shen, and Yong Jae Lee. 2024. Llava-next: Improved reasoning, ocr, and world knowledge.
- [36] Haotian Liu, Chunyuan Li, Qingyang Wu, and Yong Jae Lee. 2023. Visual Instruction Tuning. *arXiv preprint arXiv:2304.08485* (2023).
- [37] Shilong Liu, Zhaoyang Zeng, Tianhe Ren, Feng Li, Hao Zhang, Jie Yang, Qing Jiang, Chunyuan Li, Jianwei Yang, Hang Su, et al. 2025. Grounding dino: Marrying dino with grounded pre-training for open-set object detection. In *European Conference on Computer Vision*. Springer, 38–55.
- [38] Yuqi Liu, Bohao Peng, Zhisheng Zhong, Zihao Yue, Fanbin Lu, Bei Yu, and Jiaya Jia. 2025. Seg-zero: Reasoning-chain guided segmentation via cognitive reinforcement. *arXiv preprint arXiv:2503.06520* (2025).
- [39] Zuyan Liu, Yuhao Dong, Ziwei Liu, Winston Hu, Jiwen Lu, and Yongming Rao. 2024. Oryx mllm: On-demand spatial-temporal understanding at arbitrary resolution. *arXiv preprint arXiv:2409.12961* (2024).
- [40] Ze Liu, Yutong Lin, Yue Cao, Han Hu, Yixuan Wei, Zheng Zhang, Stephen Lin, and Baining Guo. 2021. Swin transformer: Hierarchical vision transformer using shifted windows. In *Proceedings of the IEEE/CVF international conference on computer vision*. 10012–10022.
- [41] Zhenhua Liu, Yunhe Wang, Kai Han, Wei Zhang, Siwei Ma, and Wen Gao. 2021. Post-training quantization for vision transformer. *Advances in Neural Information Processing Systems* 34 (2021), 28092–28103.
- [42] I Loshchilov. 2017. Decoupled weight decay regularization. *arXiv preprint arXiv:1711.05101* (2017).
- [43] Haoyu Lu, Wen Liu, Bo Zhang, Bingxuan Wang, Kai Dong, Bo Liu, Jingxiang Sun, Tongzheng Ren, Zhuoshu Li, Hao Yang, et al. 2024. Deepseek-vl: towards real-world vision-language understanding. *arXiv preprint arXiv:2403.05525* (2024).
- [44] Gen Luo, Yiyi Zhou, Xiaoshuai Sun, Liujuan Cao, Chenglin Wu, Cheng Deng, and Rongrong Ji. 2020. Multi-task collaborative network for joint referring expression comprehension and segmentation. In *Proceedings of the IEEE/CVF Conference on computer vision and pattern recognition*. 10034–10043.
- [45] Yiwei Ma, Zhibin Wang, Xiaoshuai Sun, Weihuang Lin, Qiang Zhou, Jiayi Ji, and Rongrong Ji. 2024. INF-LLaVA: Dual-perspective Perception for High-Resolution

- Multimodal Large Language Model. *arXiv preprint arXiv:2407.16198* (2024).
- [46] Junhua Mao, Jonathan Huang, Alexander Toshev, Oana Camburu, Alan L Yuille, and Kevin Murphy. 2016. Generation and comprehension of unambiguous object descriptions. In *Proceedings of the IEEE conference on computer vision and pattern recognition*. 11–20.
- [47] AI Meta. 2024. Introducing meta llama 3: The most capable openly available llm to date. *Meta AI* (2024).
- [48] R OpenAI. 2023. Gpt-4 technical report. arxiv 2303.08774. *View in Article* 2, 5 (2023).
- [49] Maxime Oquab, Timothée Darcet, Théo Moutakanni, Huy Vo, Marc Szafraniec, Vasil Khalidov, Pierre Fernandez, Daniel Haziza, Francisco Massa, Alaaeldin El-Nouby, et al. 2023. Dinov2: Learning robust visual features without supervision. *arXiv preprint arXiv:2304.07193* (2023).
- [50] Vignesh Ramanathan, Anmol Kalia, Vladan Petrovic, Yi Wen, Baixue Zheng, Baishan Guo, Rui Wang, Aaron Marquez, Rama Kovvuri, Abhishek Kadian, et al. 2023. Paco: Parts and attributes of common objects. In *Proceedings of the IEEE/CVF Conference on Computer Vision and Pattern Recognition*. 7141–7151.
- [51] Hanoona Rasheed, Muhammad Maaz, Sahal Shaji, Abdelrahman Shaker, Salman Khan, Hisham Cholakkal, Rao M Anwer, Eric Xing, Ming-Hsuan Yang, and Fahad S Khan. 2024. Glamm: Pixel grounding large multimodal model. In *Proceedings of the IEEE/CVF Conference on Computer Vision and Pattern Recognition*. 13009–13018.
- [52] Zhongwei Ren, Zhicheng Huang, Yunchao Wei, Yao Zhao, Dongmei Fu, Jiashi Feng, and Xiaojie Jin. 2024. Pixelm: Pixel reasoning with large multimodal model. In *Proceedings of the IEEE/CVF Conference on Computer Vision and Pattern Recognition*. 26374–26383.
- [53] InternLM Team. 2023. Internlm: A multilingual language model with progressively enhanced capabilities.
- [54] Hugo Touvron, Thibaut Lavril, Gautier Izacard, Xavier Martinet, Marie-Anne Lachaux, Timothée Lacroix, Baptiste Rozière, Naman Goyal, Eric Hambro, Faisal Azhar, et al. 2023. LLaMA: open and efficient foundation language models. *arXiv preprint arXiv:2302.13971* (2023).
- [55] Michael Tschanen, Alexey Gritsenko, Xiao Wang, Muhammad Ferjad Naeem, Ibrahim Alabdulmohsin, Nikhil Parthasarathy, Talfan Evans, Lucas Beyer, Ye Xia, Basil Mustafa, et al. 2025. Siglip 2: Multilingual vision-language encoders with improved semantic understanding, localization, and dense features. *arXiv preprint arXiv:2502.14786* (2025).
- [56] Junchi Wang and Lei Ke. 2024. LLM-Seg: Bridging Image Segmentation and Large Language Model Reasoning. In *Proceedings of the IEEE/CVF Conference on Computer Vision and Pattern Recognition*. 1765–1774.
- [57] Peng Wang, Shuai Bai, Sinan Tan, Shijie Wang, Zhihao Fan, Jinze Bai, Keqin Chen, Xuejing Liu, Jialin Wang, Wenbin Ge, et al. 2024. Qwen2-vl: Enhancing vision-language model's perception of the world at any resolution. *arXiv preprint arXiv:2409.12191* (2024).
- [58] Wenhai Wang, Zhe Chen, Xiaokang Chen, Jiannan Wu, Xizhou Zhu, Gang Zeng, Ping Luo, Tong Lu, Jie Zhou, Yu Qiao, et al. 2023. Visionllm: Large language model is also an open-ended decoder for vision-centric tasks. *Advances in Neural Information Processing Systems* 36 (2023), 61501–61513.
- [59] XuDong Wang, Shaolun Zhang, Shufan Li, Konstantinos Kallidromitis, Kehan Li, Yusuke Kato, Kazuki Kozuka, and Trevor Darrell. 2024. SegLLM: Multi-round Reasoning Segmentation. *arXiv preprint arXiv:2410.18923* (2024).
- [60] Zhaoqing Wang, Yu Lu, Qiang Li, Xunqiang Tao, Yandong Guo, Mingming Gong, and Tongliang Liu. 2022. Cris: Clip-driven referring image segmentation. In *Proceedings of the IEEE/CVF conference on computer vision and pattern recognition*. 11686–11695.
- [61] Cong Wei, Yujie Zhong, Haoxian Tan, Yingsen Zeng, Yong Liu, Zheng Zhao, and Yujia Yang. 2024. InstructSeg: Unifying Instructed Visual Segmentation with Multi-modal Large Language Models. *arXiv preprint arXiv:2412.14006* (2024).
- [62] Jiannan Wu, Muyan Zhong, Sen Xing, Zeqiang Lai, Zhaoyang Liu, Wenhai Wang, Zhe Chen, Xizhou Zhu, Lewei Lu, Tong Lu, et al. 2024. VisionLLM v2: An End-to-End Generalist Multimodal Large Language Model for Hundreds of Vision-Language Tasks. *arXiv preprint arXiv:2406.08394* (2024).
- [63] Zhuofan Xia, Dongchen Han, Yizeng Han, Xuran Pan, Shiji Song, and Gao Huang. 2024. Gsva: Generalized segmentation via multimodal large language models. In *Proceedings of the IEEE/CVF Conference on Computer Vision and Pattern Recognition*. 3858–3869.
- [64] Cilin Yan, Haochen Wang, Shilin Yan, Xiaolong Jiang, Yao Hu, Guoliang Kang, Weidi Xie, and Efstratios Gavves. 2024. Visa: Reasoning video object segmentation via large language models. In *European Conference on Computer Vision*. Springer, 98–115.
- [65] An Yang, Baosong Yang, Binyuan Hui, Bo Zheng, Bowen Yu, Chang Zhou, Chengpeng Li, Chengyuan Li, Dayiheng Liu, Fei Huang, et al. 2024. Qwen2 technical report. *arXiv preprint arXiv:2407.10671* (2024).
- [66] Senqiao Yang, Tianyuan Qu, Xin Lai, Zhuotao Tian, Bohao Peng, Shu Liu, and Jiaya Jia. 2023. LISA++: An Improved Baseline for Reasoning Segmentation with Large Language Model. *arXiv preprint arXiv:2312.17240* (2023).
- [67] Yuqi Yang, Peng-Tao Jiang, Jing Wang, Hao Zhang, Kai Zhao, Jinwei Chen, and Bo Li. 2024. Empowering Segmentation Ability to Multi-modal Large Language Models. *arXiv preprint arXiv:2403.14141* (2024).
- [68] Zhao Yang, Jiaqi Wang, Yansong Tang, Kai Chen, Hengshuang Zhao, and Philip HS Torr. 2022. Lavt: Language-aware vision transformer for referring image segmentation. In *Proceedings of the IEEE/CVF Conference on Computer Vision and Pattern Recognition*. 18155–18165.
- [69] Ting Yao, Yehao Li, Yingwei Pan, Yu Wang, Xiao-Ping Zhang, and Tao Mei. 2023. Dual vision transformer. *IEEE transactions on pattern analysis and machine intelligence* 45, 9 (2023), 10870–10882.
- [70] Jiabo Ye, Anwen Hu, Haiyang Xu, Qinghao Ye, Ming Yan, Guohai Xu, Chenliang Li, Junfeng Tian, Qi Qian, Ji Zhang, et al. 2023. Ureader: Universal ocr-free visually-situated language understanding with multimodal large language model. *arXiv preprint arXiv:2310.05126* (2023).
- [71] Ao Zhang, Yuan Yao, Wei Ji, Zhiyuan Liu, and Tat-Seng Chua. 2023. Next-chat: An lmm for chat, detection and segmentation. *arXiv preprint arXiv:2311.04498* (2023).
- [72] Hao Zhang, Feng Li, Shilong Liu, Lei Zhang, Hang Su, Jun Zhu, Lionel M Ni, and Heung-Yeung Shum. 2022. Dino: Detr with improved denoising anchor boxes for end-to-end object detection. *arXiv preprint arXiv:2203.03605* (2022).
- [73] Tao Zhang, Xiangtai Li, Hao Fei, Hao Bo Yuan, Shengqiong Wu, Shunping Ji, Chen Change Loy, and Shuicheng Yan. 2024. Omg-llava: Bridging image-level, object-level, pixel-level reasoning and understanding. *arXiv preprint arXiv:2406.19389* (2024).
- [74] Lianmin Zheng, Wei-Lin Chiang, Ying Sheng, Siyuan Zhuang, Zhanghao Wu, Yonghao Zhuang, Zi Lin, Zhuohan Li, Dacheng Li, Eric Xing, et al. 2023. Judging llm-as-a-judge with mt-bench and chatbot arena. *Advances in Neural Information Processing Systems* 36 (2023), 46595–46623.
- [75] Rongkun Zheng, Lu Qi, Xi Chen, Yi Wang, Kun Wang, Yu Qiao, and Hengshuang Zhao. 2024. ViLLa: Video Reasoning Segmentation with Large Language Model. *arXiv preprint arXiv:2407.14500* (2024).
- [76] Bolei Zhou, Hang Zhao, Xavier Puig, Sanja Fidler, Adela Barriuso, and Antonio Torralba. 2017. Scene parsing through ade20k dataset. In *Proceedings of the IEEE conference on computer vision and pattern recognition*. 633–641.
- [77] Chenchen Zhu, Fanyi Xiao, Andrés Alvarado, Yasmine Babaei, Jiabo Hu, Hichem El-Mohri, Sean Culatana, Roshan Sumbaly, and Zhicheng Yan. 2023. Egoobjects: A large-scale egocentric dataset for fine-grained object understanding. In *Proceedings of the IEEE/CVF International Conference on Computer Vision*. 20110–20120.
- [78] Deyao Zhu, Jun Chen, Xiaoqian Shen, Xiang Li, and Mohamed Elhoseiny. 2023. Minigpt-4: Enhancing vision-language understanding with advanced large language models. *arXiv preprint arXiv:2304.10592* (2023).
- [79] Xueyan Zou, Zi-Yi Dou, Jianwei Yang, Zhe Gan, Linjie Li, Chunyuan Li, Xiyang Dai, Harkirat Behl, Jianfeng Wang, Lu Yuan, et al. 2023. Generalized decoding for pixel, image, and language. In *Proceedings of the IEEE/CVF Conference on Computer Vision and Pattern Recognition*. 15116–15127.
- [80] Xueyan Zou, Jianwei Yang, Hao Zhang, Feng Li, Linjie Li, Jianfeng Wang, Lijuan Wang, Jianfeng Gao, and Yong Jae Lee. 2024. Segment everything everywhere all at once. *Advances in Neural Information Processing Systems* 36 (2024).